

Combined Investigation of Water Sorption on TiO₂ Rutile (110) Single Crystal Face: XPS vs. Periodic DFT

H. Perron^{1,2}, J. Vandendorre², C. Domain¹, R. Drot², J. Roques², E. Simoni²,
J.-J. Ehrhardt³, and H. Catalette¹

¹ EDF-R&D, Département Matériaux et Mécanique des Composants, Les Renardières, Ecuelles, F-77818 Moret-sur-Loing Cedex, France.

² IPN Orsay UMR 8608 - Université Paris XI, Bâtiment 100, F-91406 Orsay Cedex, France.

³ LCPME UMR 7564 CNRS - Université Henri Poincaré, Nancy I, 405 rue de Vandoeuvre, F-54600 Villers-lès-Nancy, France.

Corresponding Author

Jérôme Roques, Université de Paris XI, Institut de Physique Nucléaire, Bâtiment 100, F-91406 Orsay Cedex, France. Tel: +33(0)169156869; Fax: +33(0)169157150; e-mail: roques@ipno.in2p3.fr

Keywords: water, sorption, rutile TiO₂, (110), XPS, DFT.

Abstract

XPS and periodic DFT calculations have been used to investigate water sorption on the TiO₂ rutile (110) face. Two sets of XPS spectra were collected on the TiO₂ (110) single crystal

clean and previously exposed to water: the first set with photoelectrons collected in a direction parallel to the normal to the surface; and the second set with the sample tilted by 70°, respectively. This tilting procedure promotes the signals from surface species and reveals that the first hydration layer is strongly coordinated to the surface and also that, despite the fact that the spectra were recorded under ultra-high vacuum, water molecules subsist in upper hydration layers. In addition, periodic DFT calculations were performed to investigate the water adsorption process to determine if molecular and/or dissociative adsorption takes place. The first step of the theoretical part was the optimisation of a dry surface model and then the investigation of water adsorption. The calculated molecular water adsorption energies are consistent with previously published experimental data and it appears that even though it is slightly less stable, the dissociative water sorption can also take place. This assumption was considered, in a second step, on a larger surface model where molecular and dissociated water molecules were adsorbed together with different ratio. It was found that, due to hydrogen bonding stabilisation, molecular and dissociated water molecules can coexist on the surface if the ratio of dissociated water molecules is less than $\approx 33\%$. These results are consistent with previous experimental works giving a 10–25 % range.

1 Introduction

During the last decade, the titanium dioxide TiO_2 has been widely studied, as well on the experimental point of view as on the theoretical one, due to its numerous applications in photochemistry and catalysis [1-5]. At the natural state, the titanium dioxide can be found under three crystallographic phases which are: rutile, anatase and brookite, in order of abundance. The rutile phase has been more extensively studied than the two others and several microscopic studies were carried out under ultra-high vacuum (UHV) conditions and

with preliminary treatments (Ar^+ -ion bombardment, irradiation, high temperature), allowing a detailed knowledge of some selected crystallographic faces at the atomic level in terms of relaxation, reconstruction and defects [6-12]. Then, many metal and metal oxide overlayer growth [13-18], organic and inorganic molecule adsorptions [19-26], have also been studied and the surface chemistry on this phase was abundantly investigated. Among the low index faces naturally present in the rutile phase powder, the (110) face was found as the most stable one [27,28] and thus has been much more studied than the others. All these experimental investigations have besides been recently reviewed by Diebold [29]. On the theoretical plan, bulk, low index faces and adsorption studies have also been performed. In particular on the rutile (110) face where small molecules (H_2O , CO , $\text{NH}_3\dots$) [30-34], atomic ions (Na^+ , K^+ , $\text{Ca}^{2+}\dots$) [35-37] or metallic atoms (Au , Cu , $\text{Ag}\dots$) [38-40] were sorbed.

In order to get structural information on the environment of the surface atoms and to determine the nature of the surface reactive groups, X-Ray Photoelectron Spectroscopy (XPS) was carried out. The mechanism of water adsorption onto the TiO_2 surface is still a matter of debate because the water sorption being described either by a molecular mechanism or by a dissociative one. Some experimental data suggests that these two mechanisms may occur simultaneously [41-43]. The powder surfaces in aqueous solutions are commonly described as hydroxylated surfaces covered by water molecules (dissociated or not) on the surface metallic atoms which complete their unsatisfied coordination. This representation seems to be a satisfactory description of the water interaction with TiO_2 rutile (110) samples [44,45]. A problem for oxide surface description, in particular on the TiO_2 (110) face, is the oxygen vacancies determination. Some authors, using XPS, have asserted that oxygen vacancies are “cured” by water molecules when the solid surfaces are in contact with the aqueous solution [44]. Others have shown evidence by XPS and Ultraviolet Photoelectron Spectroscopy (UPS) that, under UHV conditions, water groups are dissociated by sorption on oxygen vacancies

[44,46,47]. In addition, Scanning Tunneling Microscopy (STM) studies [46,48] show that under UHV condition, water sorbs preferentially on defects due to the reconstruction of the (110) face. From Temperature Programmed Desorption (TPD) experiments [43,49,50], hydroxyl groups appeared on the TiO₂ (110) surface at 300 K and are eliminated for temperature higher than 500 K. The molecular sorption energy was evaluated to 17–19 and 11–24 kcal/mol using TPD and Modulated Beams respectively [43,51,52], while no energetic information is available for the dissociated form.

In this work, both experimental and theoretical studies were performed in order to get some insight on the reactive surface sites and then clarify if the TiO₂ rutile (110) face should be considered as an hydroxylated surface with H₂O and/or OH groups. This first step should lead to a better understanding of the TiO₂ rutile (110) / water interface in order to further study the uranyl sorption process on this substrate [53-55]. In the first part, the TiO₂ rutile (110) face was investigated using XPS in order to characterise the surface species. Then, periodic Density Functional Theory (DFT) calculations were performed on the dry and the hydrated TiO₂ rutile (110) face. Finally, the coadsorption of molecular and dissociated water molecules was studied to determine in what extent the water dissociation can occurs on this substrate.

2 Techniques

2.1 Angle-Resolved XPS

The titanium dioxide rutile (110) single crystal, purchased by CERAC, was 1x10x10 mm³ in size. The hydration experiments were carried out, at room temperature in batch mode, in polypropylene tubes. The single crystal was hydrated in a NaClO₄ 0.1 M solution (the Na⁺

and ClO_4^- are known to do not react with the surface) at $\text{pH} = 3.0$ for 24 hours. The single crystal was then taken off from the solution, washed with distilled water to remove background salt and finally dried at room temperature. Kinetic measurements have already shown that the hydration equilibrium is reached under these experimental conditions.

The O1s XPS spectra are collected by an XPS apparatus (KRATOS analytical) with a KRATOS AXIS Ultra DLD (Delay Lines Detector) multidetection electron analyser working in a Fixed Analyser Transmission (FAT) mode. The source of photons is a monochromatized $\text{AlK}\alpha$ lamp producing an incident X-ray beam at 1486.69 eV with a FWHM (Full-Width Half-Maximum) of 0.26 eV. The single crystal sample, hold on a metallic plate, is analysed in a chamber under 10^{-9} mbar vacuum. Moreover, this apparatus allows to tilt the oriented single crystal in order to enhance the signal corresponding to the outermost atomic layers, and therefore to separate the surface and bulk contributions in the photoelectron spectra. The O1s peaks are recorded at $\text{FAT} = 20$ eV, due to the poor electrical conductivity of this oxide, the charge neutraliser is used and the charge effects are corrected using the C1s line of the adventitious carbon at 284.6 eV. The angle-resolved XPS spectra are fitted with the software XPSPeak3.0 program [56], using a Gaussian-Lorentzian peak shape with a Shirley baseline as background. The binding energy precision is about 0.2 eV, and the FWHM corresponding to the O1s component is 1.3 eV.

2.2 Computational Details

All DFT periodic calculations were performed using the Vienna *ab initio* Simulation Package, VASP 4.6 [57-60], using the generalized gradient approximation (GGA) formalism as defined by Perdew and Wang [61], for the exchange-correlation energy evaluation. All atoms were described with pseudopotentials taken from the VASP library and developed on plane waves

basis sets using the Projector Augmented Wave (PAW) method [62,63]. Titanium atoms were described with four valence electrons ($4s^23d^2$), oxygen ones with six electrons ($2s^22p^4$) and hydrogen atoms with one electron ($1s^1$). The Brillouin zone was integrated using the Monkhorst-Pack sets of k-points [64], centered at the Γ point, depending on the supercell dimensions and on the number of atoms. Results for bulk relaxations were checked for convergence with respect to the number of k-points as well as the energy cutoff. Except for calculating bulk parameters, all atomic relaxations were performed at constant volume (at the bulk equilibrium lattice parameters) by using the conjugate gradient optimisation scheme. The (110) face was built from direct bulk cleavage and exhibit undercoordinated atoms relative to bulk structure. Water molecules were introduced on only one side of the slabs.

3 Experimental Results and Discussion

First, O1s XPS spectra were collected in a direction normal to the (110) single crystal face (Fig. 1-a). In such experimental conditions, three components are clearly observed, located at 529.7, 531.0 and 532.2 eV, respectively. The major contribution arises from the bulk O^{2-} oxygen atoms, located at 529.7 eV, which is the value usually reported for TiO_2 samples. Thus, the two other components should correspond to surface groups. In order to verify this assumption, the sample was tilted by 70° (Fig. 1-b). A fourth component, located at 533.5 eV, is observed (Table I). Therefore, by comparing the two spectra, it is possible to unambiguously identify the surface groups since their relative intensities are enhanced by the tilting process. As the relative intensities of the 531.0, 532.2 and 533.5 eV contributions are strongly promoted by the crystal rotation, they are assigned to surface species. The peaks located at 531.0 eV and 532.2 eV are observed either for the photoelectrons collection along the normal of the sample or at grazing angle of detection. According to the literature

[45,65,66], they can be addressed to the two-fold and to single-fold oxygen atoms, respectively. The weakest contribution (533.5 eV), only observed for the tilted sample, could be tentatively attributed to the oxygen of molecular physisorbed water molecules (upper-hydration layer). Indeed, the main part of this layer is evacuated under UHV (10^{-9} mbar) due to the value of the enthalpy of adsorption around 10 kcal/mol [67]; therefore it is expected that this contribution should be weak which is actually observed (see Fig. 1-b).

Therefore, the angle-resolved XPS experiments suggest strongly that three kinds of oxygen atoms could be present on the TiO_2 (110) surface namely: three-fold near surface oxygen atoms (noted Os) which are almost identical to bulk ones (529.7 eV); two-fold ones, refer as “bridging” oxygen atoms (531.0 eV) and single-fold ones, denoted “terminal” oxygen (532.2 eV). This assumption is consistent with the number of titanium atoms surrounding the oxygen surface species: the lower the number of titanium atoms, the higher the binding energy. However, the assignation of the various components of the O1s peaks proposed above does not provide unambiguous information on the protonation state of the surface oxygen atoms (saturated with none, one or two hydrogen atoms). Then, theoretical calculations were carried out to address this point.

4 Bulk Rutile and Dry (110) Face

4.1 Bulk

The theoretical part of this study started by optimising the rutile bulk parameters in order to build the (110) face and to determine the accuracy of the modelling. These first calculations were performed using different sets of k-points and energy cutoff to evaluate their effects on the bulk parameters and to optimise them. The bulk rutile unit cell is tetragonal with $a = b =$

4.587 Å, $c = 2.954$ Å, internal parameter $x = 0.305$ and $c/a = 0.644$ ([68] and references therein). The optimised parameters (see Table II) were obtained with a $5 \times 5 \times 5$ k-point mesh and a 350 eV cutoff. These calculated parameters ($a = b = 4.649$ Å, $c = 2.972$ Å, internal parameter $x = 0.304$ and $c/a = 0.640$) are close to the experimental ones and agree with previous theoretical works (see Table 2). They have thus been used for all calculations in this study. In addition, it has been checked that the (110) face was found as the most stable one.

4.2 Dry (110) Face

According to Jones *et al.* [69,70], three major crystallographic faces were identified in rutile powders: (110), (101) and (100) with respectively the ratio 60% / 20% / 20%. The dry TiO₂ rutile (110) face (Fig. 2) exhibits atoms with different environments. First, a pentacoordinated titanium atom, noted Ti(5), with an unsaturated valence and known as a Lewis acidic site. There are also two kinds of oxygen atoms, the first one is localised in the surface plane and is threefold coordinated (noted Os); the second is prominent from the surface by about 1 Å and is only doubly coordinated (noted Ob for “bridging” oxygen) and can be considered as a Lewis basic site. Surface energies were calculated using Eq. 1:

$$E_{surf} = \frac{E_{slab} - E_{TiO_2} N_{TiO_2}}{2S}, \quad (1)$$

where E_{slab} is the total energy of the supercell, E_{TiO_2} the reference energy for a TiO₂ unit in bulk phase, N_{TiO_2} the number of TiO₂ unit in the supercell and S the surface area of one side of the slab (the unit area being here $a\sqrt{2} \times c$). Here, a layer (L) is defined as a plane containing titanium and oxygen atoms, each separated by a $(\frac{a\sqrt{2}}{2})$ distance. All (110) surface energies were obtained using a $3 \times 1 \times 5$ k-point grid (the system being

$a\sqrt{2} \times (nL + vacuum) \times c$). In agreement with Bates *et al.* calculations [71], it was determined that a ($a\sqrt{2}$) vacuum thickness is enough to neglect the interaction between two neighbouring slabs.

4.2.1 Slab Thickness

In order to determine the converged surface energy, calculations with slabs composed from 3 to 13 layers were performed (see “Fully Relaxed” in Fig. 3). All atomic positions were able to relax during these calculations. As already noted by Bates *et al.* [71] and Bredow *et al.* [72] the surface energy oscillates with the number of layers used in the models. However, the amplitude of these fluctuations decreases when the number of layers increases. Convergence was reached (within 0.01 J/m²) from 10–12 layer systems (see Fig. 3). Referring to the converged surface energy, even nL give smaller values and odd nL lead to bigger ones. To explain these weakened oscillations, a scheme based on nL parity and surface relaxation is proposed. Fig. 4-a represents the experimental relaxation of the most external layer of the TiO₂ (110) surface relative to bulk positions (in light). The Ti(5) atoms fall down into the surface and the Ob atoms get closer to the surface that adopt a kind of “sawtooth” profile. This rumpling relaxation can be explained by a covalent character of the Ti–O bonds: it is easier to bend than to modify their length [73]. According to this scheme, the relaxation of a 2L slab is represented on Fig. 4-b. In this case, the relaxation of both sides are correlated and suit perfectly. There is absolutely no constraint, leading to an “over-relaxation” for the two surfaces of the 2L slab, the surface energy is very low. Then, for the 3L slab (Fig. 4-c), a problem occurs for the central layer because its relaxation can not match simultaneously with that of the two external layers. This disagreement implies no relaxation for this central layer (Fig. 4-d) leading to an “under-relaxation” of the two sides and thus to a higher surface energy. However, when nL increases, the relaxations of each side are less and less correlated

and the surface energy converges progressively until 0.50 J/m². Atom displacements, due to the surface relaxation, are of different amplitude according to nL but remain in agreement with experimental [6,7] and theoretical [71,74-78] observations. On the surface, the Ti–O bonds lengths are modified relative to the two bulk ones (1.97 and 2.00 Å): d(Ti(6)–Ob) = 1.85 Å, d(Ti(6)–Os) = 2.05 Å. It was also previously underlined that the Ti(5) atom falls down into the surface leading to a short bond length with the oxygen atom located below at 1.83 Å. The calculated surface energies found in the literature are larger with PW91 (0.73 [71], 0.81 [74]) and Becke-Perdew (BP) (0.84 [79] J/m²), while Lazzeri *et al.* PBE calculations lead to a smaller value (0.31 J/m² [80,81]). These differences are not only due to the exchange-correlation functional but also to the pseudopotentials used.

4.2.2 Internal Constraints

Following these previous observations, internal constraints were added in the slabs to isolate the relaxation of each side. These constraints should reduce the influence of nL parity and thus allow to reach convergence for weaker slabs thicknesses. During the relaxation process, some of the most internal layers of the slabs were frozen to atomic bulk positions. As an example, for a 5L slab, if the most central layer is frozen, two layers on both sides will be able to relax, while if the three most internal layers are frozen, only one layer on both sides will relax. These slabs with internal constraints were noted nL_m, where nL is the total number of layers and m the number of optimised external layers on each side of the slab. The surface energies of the unrelaxed systems were also calculated as reference points. Surface energies of these constrained systems are reported in Fig. 3. For the most constrained systems (Unrelaxed), the surface energies are larger by about 0.8–0.9 J/m² relative to totally unconstrained ones (Fully relaxed), but nL parity has smaller effects. By unconstraining slightly these systems (nL₁), the surface energies decrease significantly by about 0.6–0.7

J/m² and the oscillations with nL parity becomes smaller. By again unconstraining these systems (nL_2), the surface energies still decrease (by about 0.1 J/m²) and remain quasi-stable with nL. For the last systems (nL_3), there is no significant difference relative to the nL_2 systems. For the three nL_m systems, surface energy convergence is here reached within 0.02 J/m² for 5–8 layer systems, even if these converged energies are slightly larger than the one of the totally unconstrained systems. In order to study large surfaces, it becomes necessary to model the system with the thinnest possible slab. Following these results on the dry rutile (110) face, a 5 layer system, with its most internal layer frozen to bulk positions (5L_2), has been chosen as an accurate surface model. Surface atom displacements are in agreement with the unconstrained systems.

5 Water Sorption on the (110) Face

According to the experimental part of this study, a new surface oxygen species is created on the dry TiO₂ rutile (110) face due to the solvent interaction (water molecules). It is generally considered that the water molecule sorption can occur following two mechanisms: a molecular one (noted M), where the water molecule is linked to the Ti(5) atom, which corresponds to the experimental “terminal O” atom doubly protonated; and a dissociative one (noted D), where an OH group is linked to the Ti(5) atom, corresponding to the experimental “terminal O” atom singly protonated, and the remaining hydrogen atom is transferred to a neighbouring O_b. Moreover, for each mechanism, the water molecule, or the two fragments, can be involved in hydrogen bonding. The periodic system arrangement used here thus leads to six different geometries (see Fig 5). These six structures, studied in this work, will be referred as X_n where X = M or D (for a molecular or a dissociative sorption) and n = 0, 1 or 2, the number of hydrogen bonds.

The sorption energies are calculated using Eq. 2:

$$E_{H_2O}^{sorbed} = E_{surface}^{dry} + E_{H_2O}^{isolated} - E_{surface}^{hydrated}, \quad (2)$$

where $E_{surface}^{dry}$ is the total energy of the surface with no water molecule, $E_{H_2O}^{isolated}$ the total energy of an isolated water molecule and $E_{surface}^{hydrated}$ the total energy of the supercell with a water molecule sorbed above a Ti(5) atom. Using Eq. 2, a positive sorption energy will be favourable. All calculations were performed with a $3 \times 1 \times 5$ k-points grid as used for the dry surfaces.

Before starting describing these six structures, some notations have to be explained (see Fig. 5). First, the oxygen atom of the added water molecule will be noted O_w if it is coordinated to two hydrogen atoms (in this case the water is molecular), whereas it will be noted O_t , for “terminal” oxygen, if one hydrogen atom has been transferred (the water is dissociated). Regarding the hydrogen atoms, they will be noted H_w if they are linked to the initial water molecule oxygen atom (O_w or O_t indifferently) while an hydrogen atom linked to an O_b one will be noted H_b .

It is known that hydrogen bonding can have huge stabilisation effects. Thus, the hydrogen bond effect was investigated to study their influence on the water sorption. Three cases were considered (with none, one or two hydrogen bonds respectively) for molecular and dissociated water. These six structures were taken as starting points. In the M_0 structure (Fig. 5-a), the water molecule plane is perpendicular to the surface and the distance between the H_w atoms and the O_b ones is large ($d > 2.60 \text{ \AA}$). Then, by breaking the symmetry, a first hydrogen bond is established with a neighbouring O_b leading to the M_1 structure (Fig. 5-c). In this case, the plane of the water molecule is still perpendicular to the surface. Finally, the coplanarity is broken by moving the remaining H_w atom out of this perpendicular plane, a second hydrogen bond is established with the O_w of the neighbouring water molecule that is sorbed on the next Ti(5) atom. This last molecular structure is the M_2 one (Fig. 5-e). The three corresponding

dissociated structures, D_0 , D_1 and D_2 , (Fig. 5-b, d and f respectively), were build in the same way to estimate the stabilisation due to the hydrogen bonds.

Several theoretical works have already been published in the literature and show contradictory results. Minot *et al.* [82,83] agree for a dissociated structure as the most stable one while Bandura *et al.* [31] or Barnard *et al.* [84] calculations lead to the molecular one. Comparing these results, it appears that the slab thickness, the surface defects and the water coverage have very important effects on the relative stabilities of the dissociated and molecular sorption of water.

5.1 Effect of the Slab Thickness

As previously showed, the surface energies oscillate with the number of layers (nL) of the slab used to model the system. Thus, it was first important to determine if the number of layers has also some effects on the water sorption energies as well on the relative stabilities of the six structures previously defined. In Table 3, the sorption energies of a water molecule on fully relaxed systems composed from 2 to 7 layers are reported.

For 2L and 4L slabs, almost all dissociated starting structures (D_0 , D_1 or D_2) lead to hydrogen-bonded molecular ones (M_1 or M_2). For the 3L slab, all the structures were stabilised and the dissociative mechanism is, in this case, always energetically more favourable, i.e. the molecular form is less stable, that is the opposite of what was just observed for the 2L and 4L slabs. Regarding the results on thicker systems, all structures have been characterised for five to seven layer systems. On 5L and 7L systems, for 0 and 1 hydrogen bond, the dissociated form is more stable than the molecular one whereas for 2 hydrogen bonds, the M_2 structure has the highest sorption energies contrary to what was observed on the 3L slabs. The results on the 6L system are consistent with those observed on the 2L and the 4L slabs.

After having noticed these differences in sorption energies with the number of layers, its influence on the different bond lengths was also studied. For the M_0 and the M_1 structure, the water molecule angle lies between 111 and 116° whereas for the M_2 structure, it remains in the range of 105 to 107° . These last values are very close to those observed in the free water molecule. This behaviour that reveals the hybridisation state of the O_w should be different between these structures: sp^2 for M_0 and M_1 and sp^3 for M_2 . The nature of the water molecule is thus not the same. For the dissociated structures (D_0 , D_1 and D_2), the $Ti(5)-O_t$ bond length oscillates between 1.90 and 1.99 \AA from two to four layer systems and then converged rapidly to $1.95 \pm 0.02 \text{ \AA}$. Regarding the molecular structures (M_0 , M_1 and M_2), the $Ti(5)-O_w$ optimised values are more dispersed with the smallest number of layers lying in a range of 2.16 to 2.34 \AA but also converged for thicker slabs to $2.25 \pm 0.02 \text{ \AA}$. In all the six structures, the $Ti(5)-O_{t/w}$ distances are always larger for even nL but the difference decrease when nL increase. Moreover, the sorption energies for odd nL are always larger which can be correlated to the surface relaxation previously discussed in § 4.2.1. Since one of the six $Ti-O$ bond is broken when the surface is built, the $Ti(5)$ atoms are undercoordinated that explains their relaxation into the surface. This relaxation should decrease their destabilisation. But, it has been demonstrated that this relaxation is not the same between odd and even nL . For even nL , what was previously qualified as an “over-relaxation”, leads to a less destabilised $Ti(5)$ than for odd nL , i.e. less reactive: the less the $Ti(5)$ is destabilised, the smaller the sorption energies are.

The effect of the number of hydrogen bonds on sorption energies is also remarkable: the stabilisation between the M_0 and the M_1 structure is around $0.1-0.2 \text{ eV}$ and $0.05-0.15 \text{ eV}$ between D_0 and D_1 . The establishment of the second hydrogen bond has a more important effect with a stabilisation of 0.3 eV between M_1 and M_2 and around 0.25 eV between D_1 and D_2 .

5.2 Effect of the Internal Constraints

It was shown in § 4.2.2 that the introduction of internal constraints stabilise the dry surface energy. These constraints should also stabilise the water molecule sorption energy with nL . The influence of the slab thickness (from 3 to 10 layers) and internal constraints on the sorption energies of the two most probable structures, M_2 (Fig. 5-e) and D_2 (Fig. 5-f), are respectively represented in Fig. 6-panel a and b.

For the M_2 structure on a fully relaxed slab (Fig. 6-a), it can be noted that, the sorption energy oscillates with the number of layers. However, as previously observed on the dry surfaces, the amplitude of these oscillations decreases with nL and the sorption energy converge slowly. The addition of the internal constraints have strong effects on the sorption energies: i) for nL_1 systems, the sorption energies are virtually linear with nL but slightly overestimated relative to the fully relaxed systems (by about 0.15 eV); ii) for nL_2 and nL_3 systems, the sorption energies are independent of nL and close to the fully relaxed ones (the difference is less than 0.05 eV). Regarding the different bond lengths, values are also greatly stabilised. For a given constraint, $Ti(5)-O_w$ values differs only by 0.02 Å, which is significantly smaller than previously observed on the fully relaxed systems (see § 5.1).

For the D_2 structure on a fully relaxed system (Fig. 6-b), the sorption energies are still oscillating with nL and the constraints have also significant effects. On nL_1 slabs, the oscillation phenomenon is greatly reduced but lead to larger sorption energies than those obtained on the fully relaxed systems. Considering the nL_2 and nL_3 systems, the calculated sorption energies stay linear with nL and are slightly overestimated relative to the fully relaxed systems.

The introduction of the constraints have also stabilised the different bond lengths. An important result is that the relative stability between the M_2 and the D_2 structure does not depend on the parity of the number of layers from five to ten. With the introduction of these constraints, the M_2 structure is always more stable than the D_2 one, even if the latter remains energetically favourable. This last aspect is very important because it shows that, due to hydrogen bonding, dissociated water molecules can be stabilised on the TiO_2 rutile (110) face and may coexist simultaneously with molecular ones. Since the relative energy between the two structures, M_2 and D_2 , is constant, the selection of a 5 to 10L layers slab should be equivalent. Nevertheless, in order to study large surface, the thinnest system has to be chosen. Following the first conclusion of the dry surface study (see § 4.2.2), it appears that the 5L slab with its most layer frozen to bulk positions (5L_2), with a M_2 structure sorption energy of 1.04 eV, should be a good hydrated surface model. This sorption energy is in agreement with Lindan *et al.* [85] calculations (0.99 eV). Moreover, the D_2 structure is only 0.13 eV less stable on this model, it is thus possible to be stabilised with hydrogen bonding. This is consistent with previous theoretical works [85,86] where “mixed” configuration (with one dissociated and one molecular water molecule on a 2×1 surface only) were tested and characterised as more stable or slightly destabilised relative to a fully molecular or dissociated coverage.

6 Partial dissociation of the first hydration layer

All previous calculations were performed with one water molecule on a (1×1) face unit area leading to a full coverage of the dissociated or of the molecular form. However, it was shown that, even if the M_2 structure is the most stable one, the D_2 one should be considered. In the following calculations, a 2×3 surface area (see Fig. 7, the supercell being

$2a\sqrt{2} \times (5L_{-2} + vacuum) \times 3c$) was used to study the energetic of the first hydration layer partially dissociated. The vacuum thickness is here $(\frac{3a\sqrt{2}}{2})$ which is enough to neglect the interaction of the water molecules with the upper slab. This supercell is composed of two hundred atoms, leading to a very big supercell what justifies the need to optimise the slab thickness while keeping an accurate description of the surface. These calculations were performed using a the Γ point because of the large supercell's dimension. The supercell with the six M_2 water molecules was taken as reference. Then, the six water molecules were progressively dissociated until having a full D_2 structure coverage. Only the most stable structures, for a given M_2 / D_2 ratio, were presented. The average destabilisation due to the partial dissociation is calculated using Eq. 3:

$$E_{destab}^{average} = \frac{E_{ref} - E_{supercell}}{N_{H_2O}^{dissociated}}, \quad (3)$$

where $E_{destab}^{average}$ is the destabilisation energy per dissociated water molecule, E_{ref} the total energy of the supercell with the six M_2 water molecules on the six Ti(5) atoms, $E_{supercell}$ the total energy of the considered supercell and $N_{H_2O}^{dissociated}$ the number of dissociated water molecules. The destabilisation of each dissociated water molecule can also be calculated using Eq. 4:

$$E_{destab}^n = E_{supercell}^{n-1} - E_{supercell}^n, \quad (4)$$

where E_{destab}^n is the destabilisation energy due to the n^{th} dissociation, $E_{supercell}^{n-1}$ the total energy of the supercell with $(n-1)$ dissociated water and $E_{supercell}^n$ the total energy of the supercell with n dissociated water. Using these equations, all calculated energies are negative because the supercells with dissociated water molecules are always less stable than the reference and supercells with less dissociated water. These energies are reported in Table IV.

Among the six supercells with dissociated water molecules, the smallest destabilisation per dissociated water molecule is observed for the 4 / 2 case (see Fig. 7). In this supercell, two dissociated water molecules are stabilised with hydrogen bonding with four molecular ones, the total destabilisation is only 0.04 eV relative to the reference which corresponds to an average destabilisation 0.02 eV or 1.9 kJ/mol per molecule or only 0.01 eV relative to the 5 / 1 case. The destabilisation energy obtained on the 5 / 1 system is also relatively small (0.03 eV or 2.9 kJ/mol). The minima should thus be located around these two cases, leading to a ratio up to 33% of dissociated water molecules in the first hydration layer (see Table IV). Regarding the average destabilisation due to the full dissociation (0 / 6 case), the calculated average value of 0.13 eV match exactly with the value previously obtained on the (1×1) surface (see § 5.2). This is the evidence that, despite the molecular form is energetically more favourable, the dissociated one could be greatly stabilised by hydrogen bonds and could thus be envisaged. This result is in agreement with experimental data where characteristic infra-red bands were detected and attributed to surface hydroxyl groups [87,88]. Moreover, some authors [52] have estimated to 10–25 % the ratio of dissociated water molecules in the first hydration layer which is consistent with the calculated range.

Conclusion

A combined investigation of water sorption on the TiO₂ rutile (110) face was performed using XPS and periodic DFT calculations. The XPS spectra recorded with the collection of the photoelectrons along the normal of the surface reveals three oxygen species. By tilting the sample, four components are detected and three of them are attributed to surface species: bridging and terminal oxygen atoms belonging directly to the surface and physi-sorbed water molecules in upper layers of hydration. Following these results, the sorption of the water

molecules was investigated using periodic DFT calculations. Before studying the sorption process itself, a dry TiO₂ rutile (110) face model was optimised with the goal to minimise its size while keeping an accurate description of the system. Internal constraints, consisting in freezing some internal layers to their atomic bulk positions, were added in order to stabilise the surface energy for relatively thin systems that allow working on larger surfaces. Then, the water sorption was studied as a function of the slab thickness and of the internal constraints: the results were consistent with those obtained on the dry surface. These two systematic studies lead to the choice of a five layer system, with its most internal layer frozen to bulk positions that should be an accurate TiO₂ rutile (110) hydrated surface model to study sorption processes. Then, it was determined that the molecular sorption of water is energetically favourable but the dissociative one can also be envisaged because it could be stabilised with hydrogen bonding. Finally, the partial dissociation of the first hydration layer was investigated by using a large 2×3 supercell with different ratios of molecular / dissociated water molecules. These simulations were performed in order to investigate if molecular and dissociated water molecules can coexist on the surface. It was found that up to 33 % of dissociated water molecules, the destabilisation due to water dissociation is greatly compensated by hydrogen bonds. This result is consistent with experimental data suggesting that 10 to 25 % of the first hydration layer could be dissociated.

Acknowledgements

The authors would like to thank Mr. J. Lambert from LCPME in Nancy for all XPS measurements. All calculations have been performed using the CEA CCRT supercomputers, in the framework of an EDF–CEA partnership, as well as the cluster of CNRS–IN2P3 in Lyon.

References

- [1] H. Onishi, Y. Iwasawa, *Phys. Rev. Lett.* 76 (1996) 791.
- [2] P. W. Murray, N. G. Condon, G. Thornton, *Phys. Rev. B* 51 (1995) 10989.
- [3] V. E. Heinrich, P. A. Cox, *The Surface Science of Metal Oxides*, Cambridge University Press, Cambridge, 1994.
- [4] C. C. Williams, J. G. Ekerdt, J. M. Jehng, F. D. Hardcastle, I. E. Wachs, *J. Phys. Chem.* 95 (1991) 8791.
- [5] G. D. Parfitt, *Croat. Chem. Acta* 45 (1973) 189.
- [6] R. Lindsay, A. Wander, A. Ernst, B. Montanari, G. Thornton, N. M. Harrison, *Phys. Rev. Lett.* 94 (2005) 246102.
- [7] G. Charlton, P. B. Howes, C. L. Nicklin, P. Steadman, J. S. G. Taylor, C. A. Muryn, S. P. Harte, J. Mercer, R. McGrath, D. Norman, T. S. Turner, G. Thornton, *Phys. Rev. Lett.* 78 (1997) 495.
- [8] J. J. Czyzewski, J. Krajniak, S. Klein, *App. Surf. Sci.* 227 (2004) 144.
- [9] U. Diebold, J. Lehman, T. Mahmoud, M. Kuhn, G. Leonardelli, W. Hebenstreit, M. Schmidt, P. Varga, *Surf. Sci.* 411 (1998) 137.
- [10] G. Charlton, P. B. Howes, C. L. Nicklin, P. Steadman, J. S. G. Taylor, C. A. Muryn, S. P. S. Fischer, A. W. Munz, K.-D. Schierbaum, W. Göpel, *Surf. Sci.* 337 (1995) 17.
- [11] P. W. Murray, N. G. Condon, G. Thornton, *Phys. Rev. B* 51 (1995) 10989.
- [12] D. Novak, E. Garfunkel, T. Gustafsson, *Phys. Rev. B* 50 (1994) 5000.
- [13] Z. Zhang, P. Fenter, L. Cheng, N. C. Sturchio, M. J. Bedzyk, M. L. Machesky, L. M. Anovitz, D. J. Wesolowski, *J. Coll. Int. Sci.* 295 (2006) 50.
- [14] S. Agnoli, M. Sambì, G. Granozzi, C. Castellarin-Cudia, S. Surnev, M. G. Ramsey, F. P. Netzer, *Surf. Sci.* 562 (2004) 150.

- [15] R. E. Tanner, I. Goldfarb, M. R. Castell, G. A. D. Briggs, *Surf. Sci* 486 (2001) 167.
- [16] S. N. Towle, G. E. Brown Jr., G. A. Parks, *J. Coll. Int. Sci.* 217 (1999) 299.
- [17] M. K. Ridley, M. L. Machesky, D. J. Wesolowski, D. A. Palmer, *Geochim. Cosmochim. Acta* 63 (1999) 3087.
- [18] P. A. O'Day, C. J. Chisholm-Brause, S. N. Towle, G. A. Parks, G. E. Brown Jr, *Geochim. Cosmochim. Acta* 60 (1996) 2515.
- [19] K. Onda, B. Li, J. Zhao, H. Petek, *Surf. Sci.* 593 (2005) 32.
- [20] M. Olsson, A.-M. Jakobsson, Y. Albinsson, *J. Coll. Int. Sci.* 266 (2003) 269.
- [21] C. Den Auwer, R. Drot, E. Simoni, S. D. Conradson, M. Gailhanou, J. Mustre de Leon, *New J. Chem.* 27 (2003) 648.
- [22] J. A. Rodriguez, J. Hrbek, Z. Chang, J. Dvorak, T. Jirsak, *Phys. Rev. B* 65 (2002) 235414.
- [23] D. Robert, S. Parra, C. Pulgarin, A. Krzton, J. V. Weber, *Appl. Surf. Sci.* 167 (2000) 51.
- [24] M. A. Henderson, *Surf. Sci.* 400 (1998) 203
- [25] A. N. Shultz, W. M. Hetherington III, D. R. Baer, L.-Q. Wang, M. H. Engelhard, *Surf. Sci.* 392 (1997) 1
- [26] K. Hadjiivanov, *Appl. Surf. Sci.* 135 (1988) 331.
- [27] H. Onishi, Y. Iwasawa, *Chem. Phys. Lett.* 226 (1994) 111.
- [28] G. D. Parfitt, *Prog. Surf. Menbr. Sci.* 11 (1976) 181.
- [29] U. Diebold, *Surf. Sci. Rep.* 48 (2003) 53.
- [30] K. Jug, N. N. Nair, T. Bredow, *Surf. Sci.* 590 (2005) 9.
- [31] A. V. Bandura, D. G. Sykes, V. Shapovalov, T. N. Troung, J. D. Kubicki, R. A. Evarestov, *J. Phys. Chem. B* 108 (2004) 7844.
- [32] C. Zhang, P. J. D. Lindan, *Chem. Phys. Lett.* 373 (2003) 15.
- [33] W. Langel, L. Menken, *Surf. Sci.* 538 (2003) 1.

- [34] M. Odelius, P. Persson, S. Lunell, *Surf. Sci.* 529 (2003) 47.
- [35] M. Předota, Z. Zhang, P. Fenter, D. J. Wesolowski, P. T. Cummings, *J. Phys. Chem. B* 108 (2004) 12061.
- [36] M. Svetina, L. Colombi Ciacchi, O. Sbaizero, S. Meriani, A. De Vita, *Acta Mater.* 49 (2001) 2169.
- [37] J. Muscat, N. M. Harrison, G. Thornton *Phys. Rev. B* 59 (1999) 15457.
- [38] Y. Wang, G. S. Hwang, *Surf. Sci.* 542 (2003) 72.
- [39] N. Lopez, J. K. Nørskov, *Surf. Sci.* 515 (2002) 175.
- [40] L. Giordano, G. Pacchioni, T. Bredow, J. F. Sanz, *Surf. Sci.* 471 (2001) 21.
- [41] P. Maksymovych, S. Mezhenny, J. T. Yates Jr., *Chem. Phys. Lett.* 382 (2003) 270.
- [42] E. L. Bullock, L. Patthey, S. G. Steineman, *Surf. Sci.* 352-354 (1996) 504.
- [43] M. A. Henderson, *Surf. Sci.*, 355 (1996) 151.
- [44] L. Q. Wang, D. R. Baer, M. H. Engelhard, A. N. Shultz, *Surf. Sci.* 344 (1995) 237.
- [45] R. L. Kurtz, R. Stockbauer, T. E. Madey, E. Roman, J. L. De Segovia, *Surf. Sci.* 218 (1989) 178.
- [46] I. M. Brookes, C. A. Muryn, and G. Thornton, *Phys. Rev. Lett.* 87 (2001) 266103.
- [47] R. Schaub, P. Thostrup, N. Lopez, E. Lægsgaard, I. Stensgaard, J. K. Nørskov, J. F. Besenbacher, *Phys. Rev. Lett.* 87 (2001) 266104.
- [48] P. Maksymovych, S. Mezhenny, and J. T. Yates Jr., *Chem. Phys. Lett.* 382 (2003) 270.
- [49] P. Maksymovych, S. Mezhenny, and J. T. Yates Jr., *Chem. Phys. Lett.* 382 (2003) 270.
- [50] M. A. Henderson, *Langmuir* 12 (1996) 5093.
- [51] M. B. Hugenschmidt, L. Gamble, C. T. Campbell, *Surf. Sci.* 302 (1994) 329.
- [52] T. Brinkley, M. Dietrich, T. Engel, P. Farrall, G. Gantner, A. Schafer, A. Szuchmacher, *Surf. Sci.* 395 (1998) 292.

- [53] H. Perron, C. Domain, J. Roques, R. Drot, E. Simoni, H. Catalette, *Radiochim. Acta*, accepted.
- [54] H. Perron, C. Domain, J. Roques, R. Drot, E. Simoni, H. Catalette, *Inorg. Chem.*, accepted.
- [55] M. Dossot, S. Crémel, J. Vandenborre, J. Grausem, B. Humbert, R. Drot, E. Simoni, *Langmuir* 22 (2006) 140.
- [56] R. W. M. Kwok, XPSPeak95, versio3.0, The Chinese University of Hong Kong, 1997.
- [57] G. Kresse, J. Hafner, *Phys. Rev. B* 47 (1993) R558.
- [58] G. Kresse, J. Hafner, *Phys. Rev. B* 49 (1994) 14251.
- [59] G. Kresse, J. Furthmüller, *Comput. Mater. Sci.* 6 (1996) 15.
- [60] G. Kresse, J. Furthmüller, *Phys. Rev. B* 54 (1996) 11169.
- [61] J. P. Perdew, Y. Wang, *Phys. Rev. B* 45 (1992) 13244.
- [62] P. E. Blöchl, *Phys. Rev. B* 50 (1994) 17953.
- [63] G. Kresse, D. Joubert, *Phys. Rev. B* 59 (1999) 1758.
- [64] H. J. Monkhorst, J. D. Pack, *Phys. Rev. B* 13 (1976) 5188.
- [65] W. Gopel, *Surf. Sci.* 139 (1984) 333.
- [66] T. K. Sham, M. S. Lazarus, *Chem. Phys. Lett.* 68 (1979) 426.
- [67] M. A. Henderson, *Surf. Sci. Rep.* 46 (2002) 1.
- [68] J. Muscat, V. Swamy, and N. M. Harrison, *Phys. Rev. B* 65 (2002) 224112.
- [69] P. Jones and J. A. Hockey, *Trans. Faraday Soc.* 67 (1971) 2669.
- [70] P. Jones and J. A. Hockey, *Trans. Faraday Soc.* 67 (1971) 2679.
- [71] S. P. Bates, G. Kresse and M. J. Gillan, *Surf. Sci.* 385 (1997) 386.
- [72] T. Bredow, L. Giordano, F. Cinquini, G. Pacchioni *Phys. Rev. B* 70 (2004) 035419.
- [73] C. Noguera, *Physics and chemistry at oxide surfaces*, Cambridge University Press, 1996, p 59.

- [74] P. J. D. Lindan, N. M. Harrison, M. J. Gillan, J. A. White, *Phys. Rev. B* 55 (1997) 15919.
- [75] M. Ramamoorthy, D. Vanderbilt, R. D. King-Smith, *Phys. Rev. B* 49 (1994) 16721.
- [76] J. Goniakowski, J. M. Holender, L. N. Kantorovich, M. J. Gillan, J. A. White, *Phys. Rev. B* 53 (1996) 957.
- [77] D. Vogtenhuber, R. Podloucky, A. Neckel, S. G. Steinemann, A. J. Freeman, *Phys. Rev. B* 49 (1994) 2099.
- [78] J. Leconte, A. Markovits, M. K. Skalli, C. Minot, A. Belmajdoub, *Surf. Sci.* 497 (2002) 194.
W. Langel, *Surf. Sci.* 496 (2002) 141.
- [79] J. Goniakowski, M. J. Gillan, *Surf. Sci.* 350 (1996) 145.
- [80] M. Lazzeri, A. Vittadini, A. Selloni, *Phys. Rev. B* 63 (2001) 155409.
- [81] M. Lazzeri, A. Vittadini, A. Selloni, *Phys. Rev. B* 65 (2002) 119901(E).
- [82] M. Menetrey, A. Markovits, C. Minot, *Surf. Sci.* 524 (2003) 49.
- [83] J. Ahdjoudj, A. Markovits, C. Minot, *Catal. Today* 50 (1999) 541.
- [84] A. S. Barnard, P. Zapol, L. A. Curtiss, *J. Chem. Theory Comput.* 1 (2005) 107.
- [85] P. J. D. Lindan, N. M. Harrison, M. J. Gillan, *Phys Rev. Lett.* 80 (1998) 762.
- [86] L. A. Harris, A. A. Quong, *Phys. Rev. Lett.* 93 (2004) 086105.
- [87] T. Bezrodna, G. Puchkovska, V. Shymanovska, J. Baran, H. Ratajczak, *J. Mol. Struct.* 700 (2004) 175.
- [88] M. Primet, P. Pichat, M.-V. Mathieu, *J. Phys. Chem.* 75 (1971) 1216.

Table I

Characteristics of O(1s) peaks on XPS spectrum of TiO₂ rutile (110) single crystal.

Binding Energy ± 0.2 (eV)	FWHM (eV)	Oxygen surface groups
529.7	1.2	Os
531.0	1.3	bridging O group
532.2	1.3	terminal O group
533.5	1.3	H ₂ O in upper layers

Table II

Optimised rutile lattice parameters (in Å) and bulk modulus (in GPa). Data from previous studies: GGA using plane waves (PW) and linear combination of atomic orbitals (LCAO) from Ref. 67. Experimental data from Ref. 67 and reference therein.

	<i>a</i>	<i>b</i>	<i>x</i>	<i>c/a</i>	<i>B</i>
Exp.	4.587	2.954	0.305	0.644	210
This Study	4.649	2.972	0.304	0.640	225
GGA (PW)	4.651	2.964	0.307	0.637	
GGA (LCAO)	4.627	2.981	0.305	0.644	

Table III

Comparison of the sorption energies (in eV) of H₂O on 2 to 7 layer systems (– = unstabilised or energetically unfavourable structure).

	M ₀ / D ₀	M ₁ / D ₁	M ₂ / D ₂
2L	0.48 / –	0.53 / –	0.82 / –
3L	0.70 / 1.15	0.91 / 1.17	1.22 / 1.39
4L	0.55 / 0.19	0.62 / 0.32	0.92 / –
5L	0.59 / 0.76	0.73 / 0.80	1.05 / 1.02
6L	0.57 / 0.29	0.65 / 0.37	0.94 / 0.65
7L	0.58 / 0.63	0.70 / 0.68	1.01 / 0.90

Table IV

Destabilisation energies per dissociated water molecule as a function of the M_2 / D_2 ratio (in eV). The percentage of dissociated water molecules is also reported.

M_2 / D_2	6 / 0	5 / 1	4 / 2	3 / 3	2 / 4	1 / 5	0 / 6
%	0	17	33	50	66	83	100
$E_{destab}^{average}$ (eV)	0.00	-0.03	-0.02	-0.06	-0.08	-0.11	-0.13
E_{destab}^n (eV)	0.00	-0.03	-0.01	-0.14	-0.13	-0.23	-0.25

Figure Captions:

Figure 1. O1s spectrum of the rutile (110) single crystal: (a) collected in a direction normal to the surface of the crystal; (b) tilted by 70° .

Figure 2. The dry TiO_2 rutile (110) face (Ti atoms in blue, O atoms in red).

Figure 3. Rutile (110) surface energy as a function of the slab thickness for 3 to 13 layer systems (in J/m^2).

Figure 4. (a) Rutile (110) face relaxation in respect to bulk positions (in light). (b) 2L slab relaxed. (c) Paradoxical relaxations on a 3L slab. (d) 3L slab relaxed.

Figure 5. The two mechanisms for a water molecule sorption on the rutile (110) face with different numbers of hydrogen bonds: (a) M_0 , (b) D_0 , (c) M_1 , (d) D_1 , (e) M_2 and (f) D_2 . Only one water molecule is represented for clarity.

Figure 6. Sorption energies (in eV) from 3L to 10L slabs with internal constraints: (a) M_2 structure and (b) D_2 structure. * The D_2 structure on the 4L fully relaxed has not been stabilised.

Figure 7. Top view of the 2×3 supercell for the 4 / 2 case. The oxygen atoms of the added water molecules are displayed in yellow colour for a better clarity.

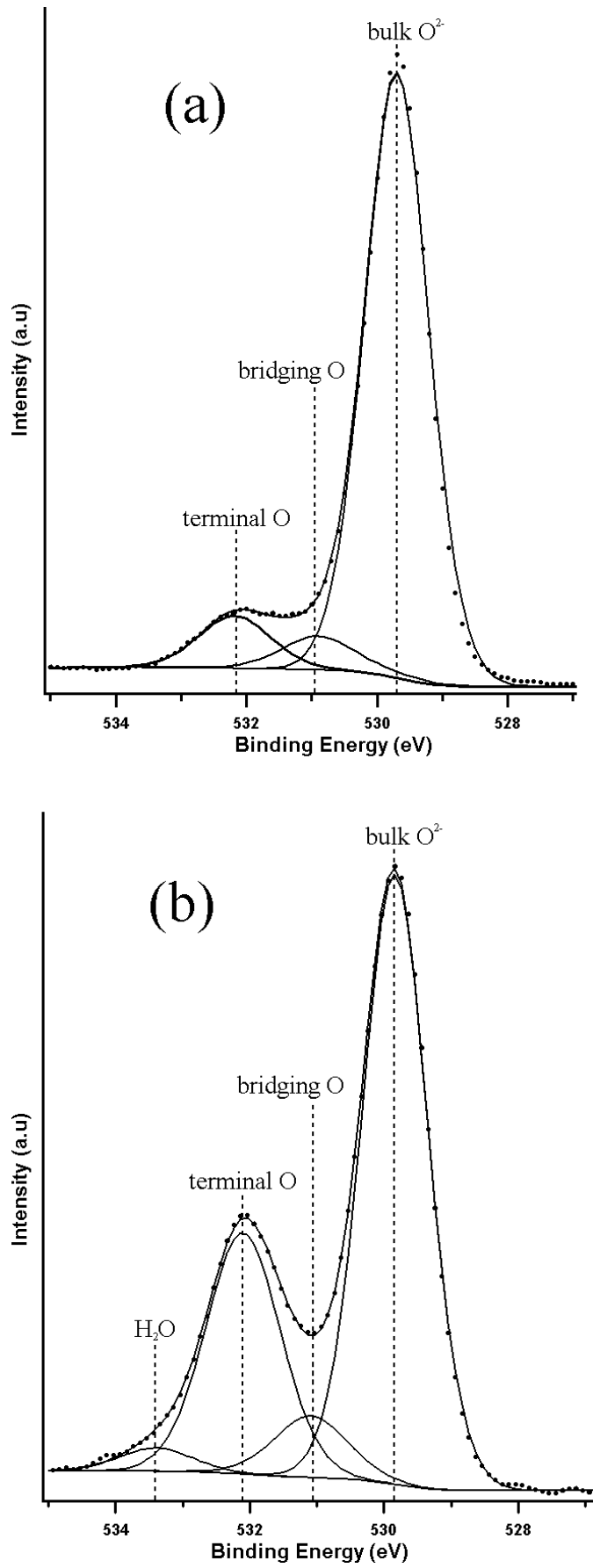


Fig. 1

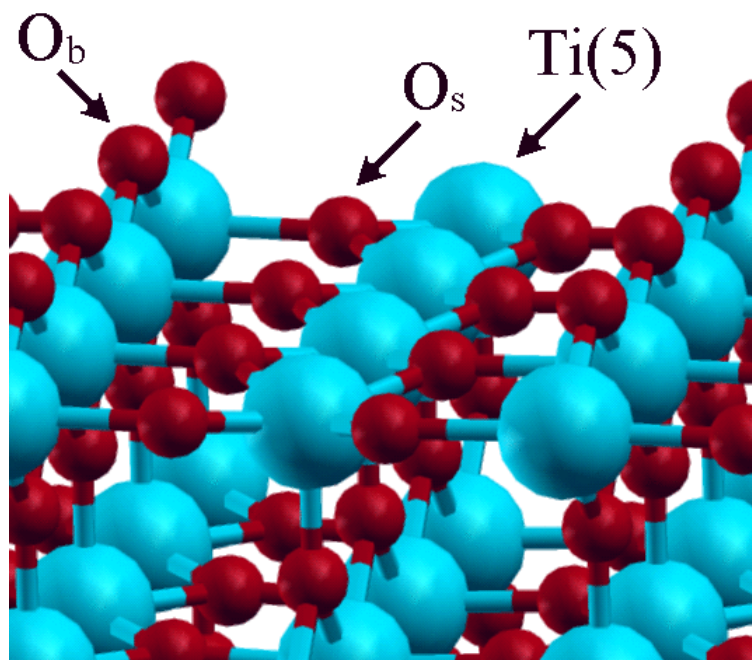


Fig. 2

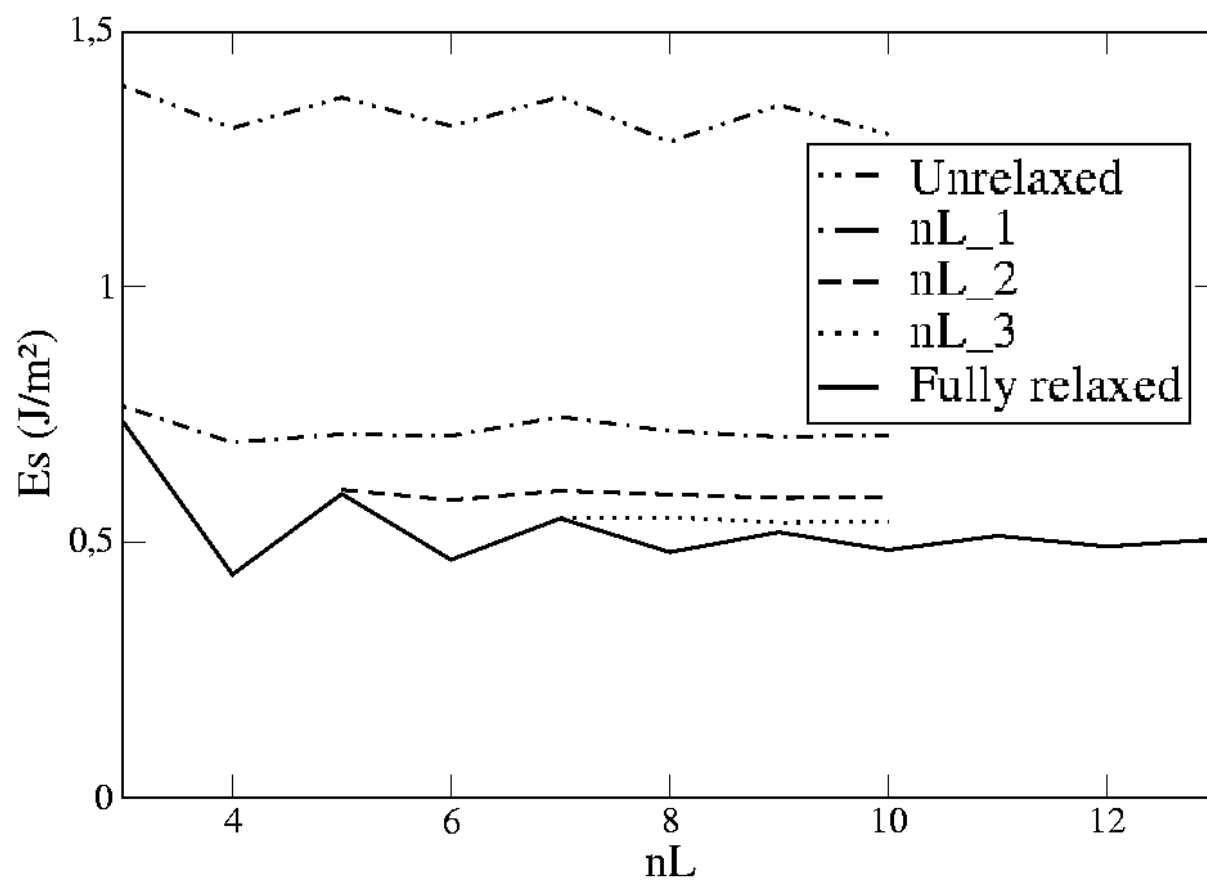


Fig. 3

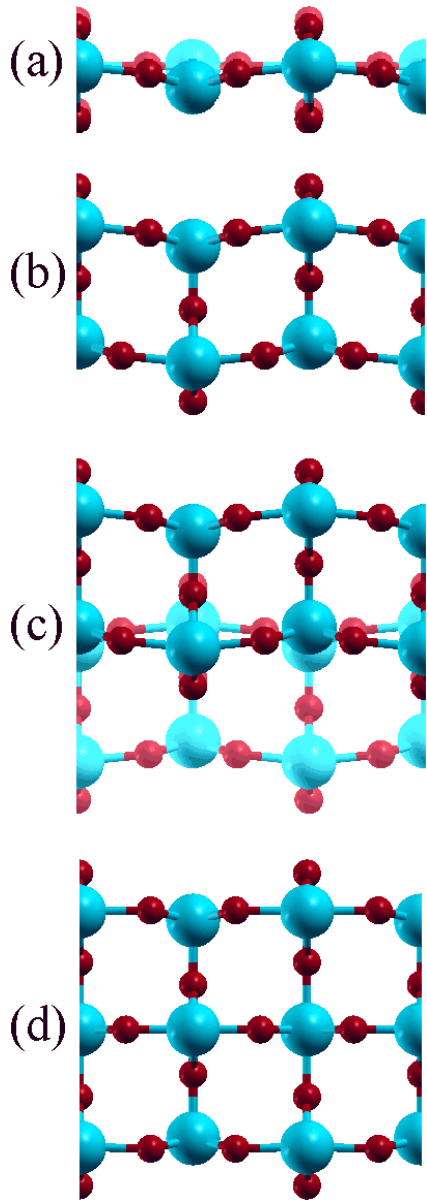


Fig. 4

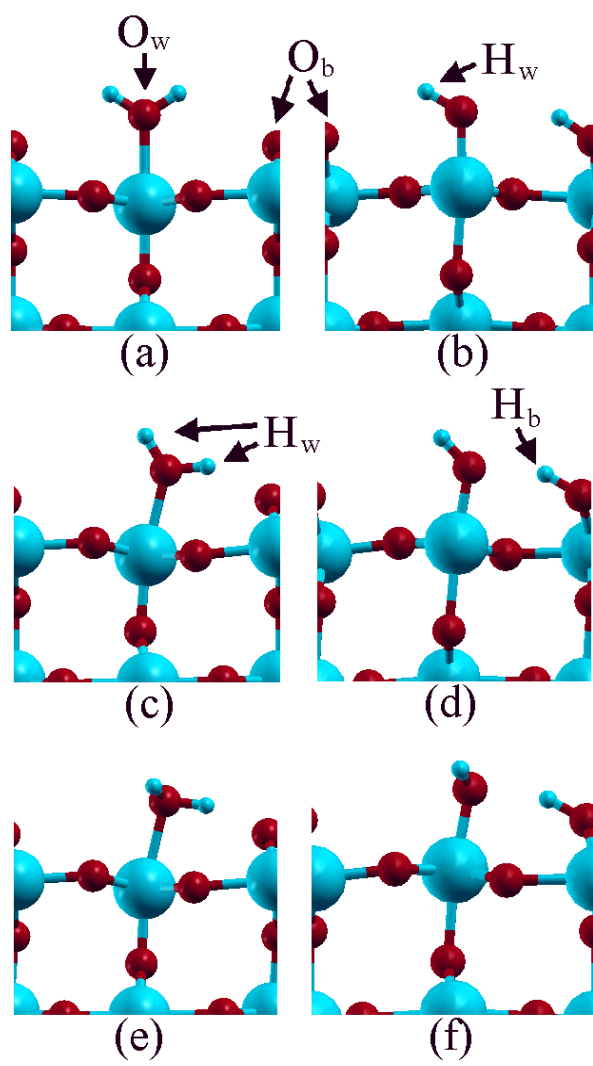


Fig. 5

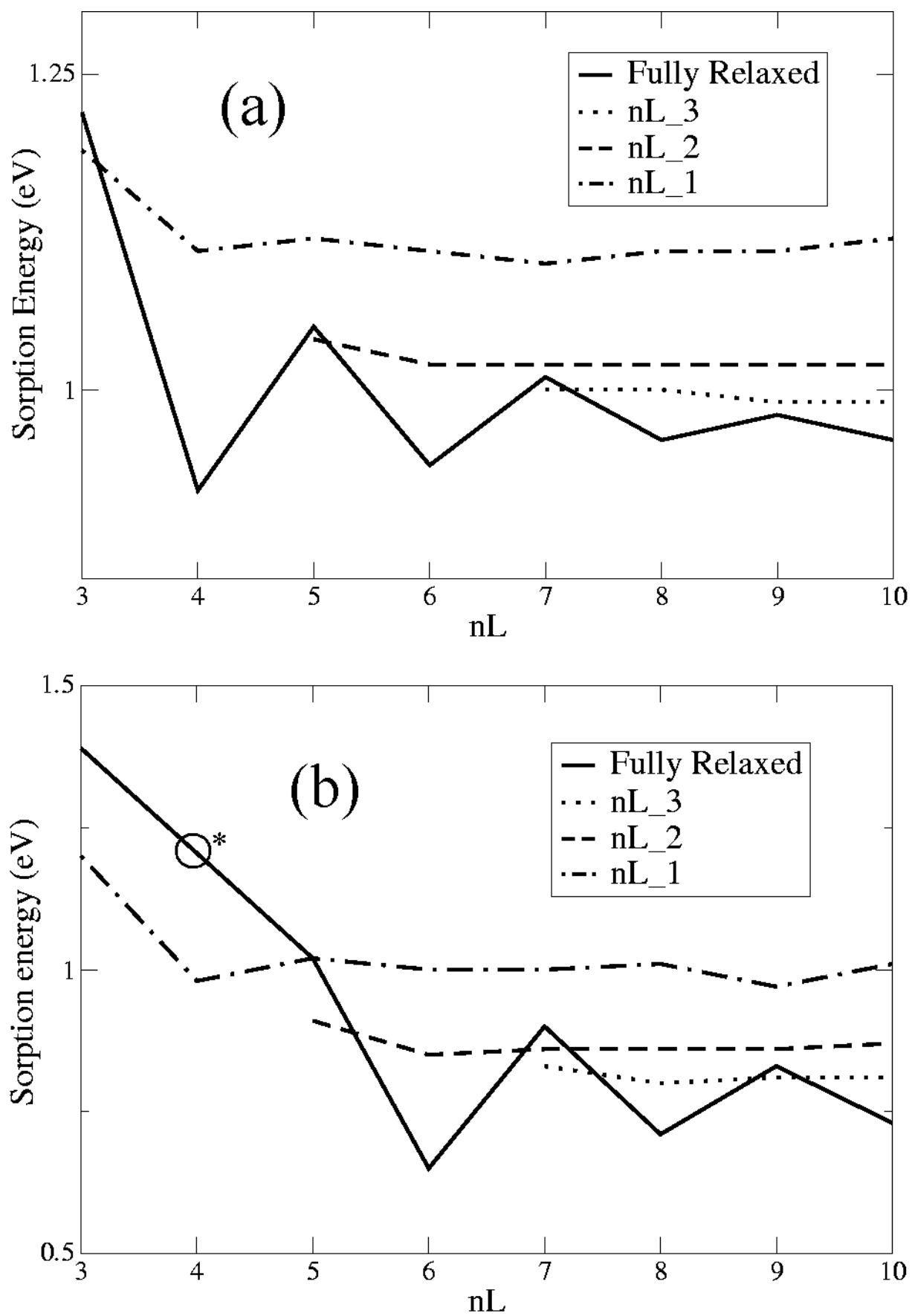


Fig. 6

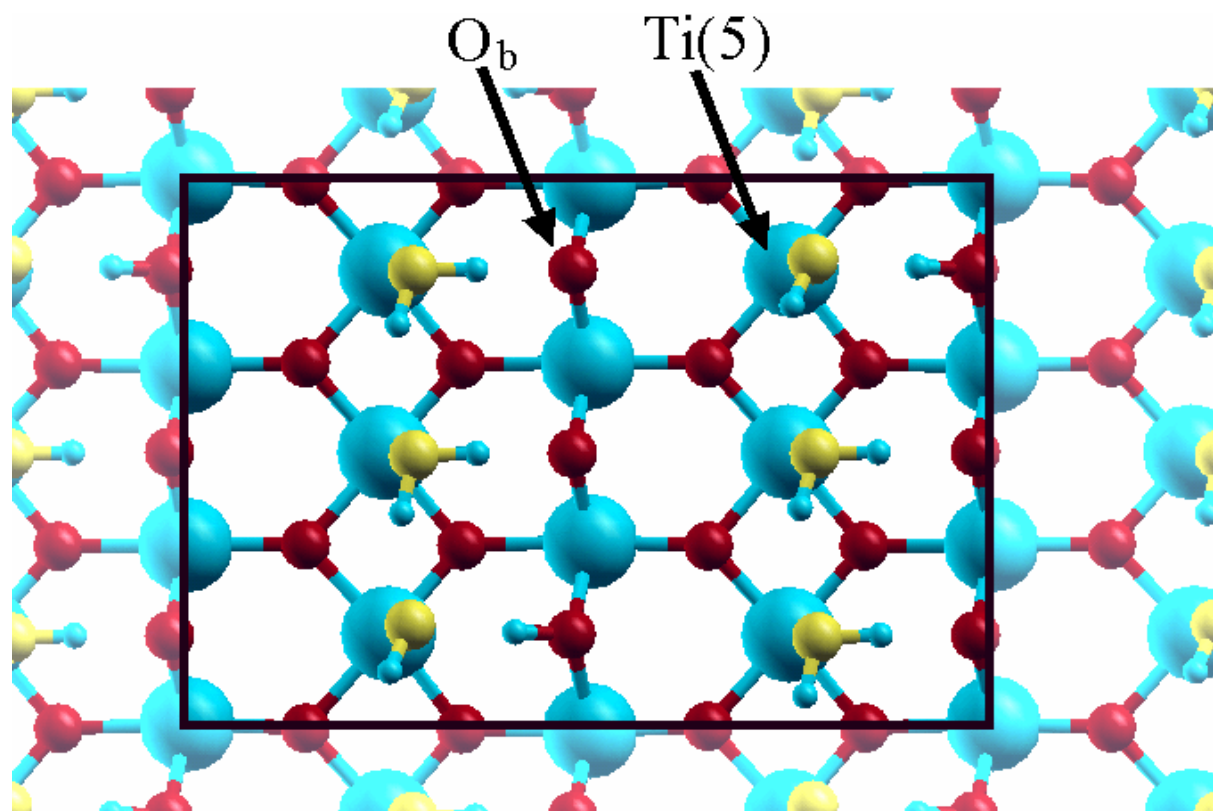


Fig. 7